Thin Solid Films 666 (2018) 6–14

Contents lists available at ScienceDirect

Thin Solid Films

journal homepage: www.elsevier.com/locate/tsf

Comparison of thickness determination methods for physical-vapor-deposited aluminum coatings in packaging applications

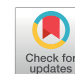

Martina Lindner[a,b,*], Florian Höflsauer[b], Julia Heider[a,b], Matthias Reinelt[b], Horst-Christian Langowski[a,b]

[a] TUM School of Life Sciences, Chair for Food Packaging Technology, Technical University of Munich, Weihenstephaner Steig 22, 85354 Freising, Germany
[b] Fraunhofer Institute for Process Engineering and Packaging IVV, Giggenhauser Straße 35, 85354 Freising, Germany

ARTICLE INFO

Keywords:
Thin film
Quartz crystal micro balance
Atomic force microscopy
Interference
Optical density
Electrical resistivity

ABSTRACT

Methods used to determine the aluminum coating thickness on polymer films may not measure the geometrical thickness directly but may instead measure the mass or other properties, thus leading to different thickness values. Common methods include the determination of evaporation rates using a quartz crystal microbalance (QCM) and the quantitative analysis of dissolved aluminum ions by inductively-coupled plasma mass spectrometry (ICP-MS), which provide mass thickness values. Alternatively, atomic force microscopy (AFM) and interference (INT) across the step of a partially removed aluminum layer yield geometrical values, and optical density (OD) and electrical resistance (ER) measure other properties. We compared the ability of these methods to determine the thickness of aluminum coatings applied to polyethylene terephthalate (PET) and paper by physical vapor deposition. We measured ER using four-point probes, five-point probes, and eddy currents. ER and OD achieved high precision but low accuracy, showing that the resistivity and absorption coefficients of thin aluminum layers can deviate from bulk constants. When the constant values were adjusted, both methods achieved higher accuracy. ICP-MS and QCM values were similar, when a geometrical model was applied, and in comparison AFM and INT showed low precision but high accuracy. When the aluminum was applied to paper instead of PET, only ICP-MS generated reliable results. In summary, the values derived using these different methods are only in agreement when method-specific constants such as absorption coefficients and resistivity are suitably modified.

1. Introduction

The thickness and consistency of aluminum coatings have a strong impact on performance. In packaging applications, performance may be defined as the effectiveness as a gas barrier or the optical impression of decorative aluminum coatings. Gas permeation has been shown to decrease with increasing aluminum thickness up to approximately 60 nm [1] and only decreases further when the coating is 1–3 orders of magnitude thicker [2,3]. However, when measuring the relationship between permeability and aluminum thickness, the values reported and the techniques used to measure the thickness of the aluminum layer varied widely [2,4–10].

Coating thickness can be measured using methods that determine mass, geometry and other properties based on parameters such as electrical conductivity, light transmission, or the quantity of aluminum ions [11], but it is unclear whether the different instruments generate equivalent values (Fig. 1). For each type of instrument, some of the factors that influence the measurement are already known, and are summarized below. More detailed information can be found elsewhere [12].

Quartz crystal microbalances (QCMs) determine the “total mass thickness” of the deposited material based on the weight of the deposited aluminum, which includes both aluminum atoms and foreign atoms such as oxygen. This technique is accurate to within ~2%, but accuracy declines with increasing aluminum thickness [13–15]. Inductively-coupled plasma mass spectrometry (ICP-MS) similarly determines the “mass thickness” but in contrast to QCM only measures the pure aluminum. This is achieved by dissolving aluminum oxide and pure aluminum in sodium hydroxide before measuring the aluminum concentration [6]. The range of detectable concentrations is limited to approximately 0.001–0.1 μg/l for aluminum in aqueous solutions [16], and the results can be affected by interference between atoms with the same *m/z* ratio [17].

Atomic force microscopy (AFM) and interference (INT) determine

* Corresponding author at: Fraunhofer Institute for Process Engineering and Packaging IVV, Giggenhauser Straße 35, 85354 Freising, Germany.
E-mail address: martina.lindner@ivv.fraunhofer.de (M. Lindner).

https://doi.org/10.1016/j.tsf.2018.09.032
Received 4 April 2018; Received in revised form 10 September 2018; Accepted 12 September 2018
Available online 15 September 2018
0040-6090/ © 2018 The Authors. Published by Elsevier B.V. This is an open access article under the CC BY-NC-ND license
(http://creativecommons.org/licenses/BY-NC-ND/4.0/).

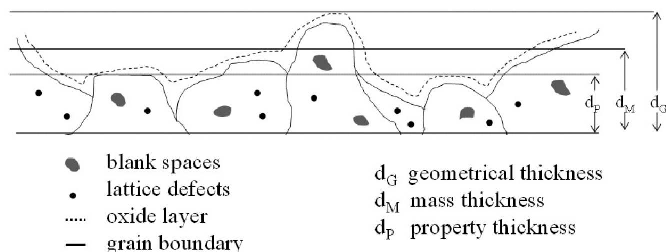

Fig. 1. Mass, geometrical and property thickness can vary widely because they are derived from diverse material characteristics such as light transmission, electrical resistance, or the quantity of metal ions.

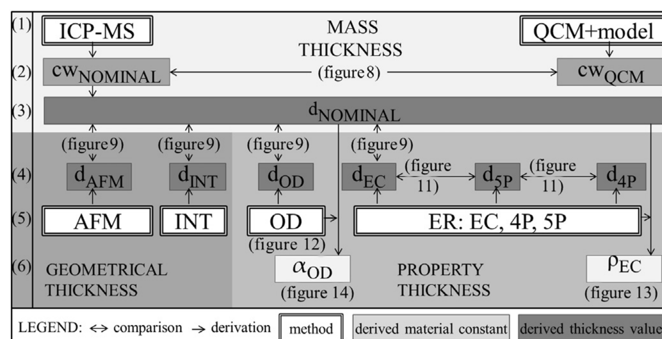

Fig. 2. Workflow for the experiments described in this article. Derivation of coating weight $cw_{NOMINAL}$ and cw_{QCM} from ICP-MS and QCM + model (1), comparison of both (2), derivation of a nominal thickness $d_{NOMINAL}$ from ICP-MS (3) and comparison of $d_{NOMINAL}$ with other methods (4,5), derivation of material constants (6) from $d_{NOMINAL}$ in combination with measured properties (5).

the "geometrical thickness" of a sample. They capture the overall thickness of aluminum and aluminum oxide on a step produced by partial removal of the deposited aluminum layer. For INT measurements, both surfaces (substrate and aluminum) are covered with an additional 10-nm gold film to equalize the reflection characteristics. If the surface is rough, the reported thickness is higher than the average thickness of the layer [18]. Similarly, AFM does not separately record inclusions and voids, and the interaction between the AFM cantilever and the surface (topography and hardness) can affect the profile and the corresponding thickness values [19].

Finally, optical density (OD) and eddy current (EC) measure an indirect "property thickness". When using the OD method, a minimum transmission of ~0.03% (OD = 3.5) is useful [20]. Although greater thicknesses can be distinguished by using more sensitive equipment, the error increases due to heterogeneities and defects. The OD also decreases over time because the light-absorbing aluminum reacts with oxygen to form transparent aluminum oxide [4]. Furthermore, the OD is defined by the absorption coefficient α and the related extinction coefficient k (see Eq. (5)), and these values are highly dependent on the process conditions, grain size, coating thickness, and wavelength of the incident light [6,21,22]. When four-point (4P) and five-point (5P) probes are used to measure the electrical resistance (ER), a variety of factors can increase the resulting values. First, the instrument's electrical contacts may scratch the surface and cause cracks in the material. Second, oxide layers with a resistivity 20 orders of magnitude higher than the pure metal can act as an isolator between the aluminum and the contacts. Third, electrons can be scattered by the surface (particularly a rough surface) and by grain and island boundaries [23–30]. When the sheet resistance is measured by contactless EC methods, the values are influenced by the presence of aluminum oxide due to its extremely high resistivity. Furthermore, the sensitivity of EC measurements also depends on many other factors, such as the properties of the electromagnetic excitation field [31–33], the sensor-to-sensor distance, and the material thickness [34].

The aim of this study was to compare the thickness measurements produced by OD, electrical sheet resistance (4P, 5P and EC), QCM, ICP-MS, AFM and INT in order to determine whether the resulting values are similar, whether any differences can be explained and whether any of the methods are affected by the substrate beneath the aluminum layer, which in this study was either the polymer polyethylene terephthalate (PET) or paper. We use the data we obtained to draw conclusions about the structure of the aluminum layer.

These are important considerations because thickness and related parameters such as gas barrier efficiency, costs, and machine speeds are regularly compared using values derived using different methods. This can lead to misunderstandings and misinterpretations, and our findings will therefore be useful for researchers working on inorganic gas barrier coatings and industrial metallizers.

The data flow in this study is summarized in Fig. 2. The thickness determined by ICP-MS was used as a reference value for all the other methods. We then determined the material constants (absorption coefficient and resistivity) from OD, ER and ICP-MS reference values in order to characterize the structure of the aluminum layer.

2. Materials and methods

2.1. Physical vapor deposition

The aluminum was applied by physical vapor deposition using an electron beam heater. The coating was applied in a 0.5 m × 1.0 m box coater (L560UV; Leybold Vacuum GmbH, Germany) at the Fraunhofer IVV (Fig. 3, right). This coater had been adapted for the roll-to-roll coating of polymer webs by adding winding equipment (deposition roll, unwinding, and rewinding; Lenze, Germany). The equipment was managed using L560 VAC Cluster Tool Controller (AIS Automation GmbH, Germany) software. The box coater was equipped with an E2M175 rotary vacuum pump (160 m^3/h) and an EH500 roots pump (505 m^3/h) both supplies by Edwards Ltd., UK, and a turbomolecular pump (850–1150 l/s, TMP 1000; Leybold Vacuum GmbH, Germany) to create a vacuum in the 10^{-4} Pa range. Remaining moisture in the chamber was extracted using a Meissner cold trap, and the deposition roll was water-cooled. The pressure was determined using a PPT-100 Pirani gauge and a HPT-100 hot cathode Bayard–Alpert–Pirani wide-range gauge, both from Pfeiffer GmbH, Germany. The EV M-10 electron beam source (270° configuration) was fitted with a Genius Carrera 10 kW high-voltage supply, all supplied by Ferrotec, Germany.

The aluminum was 99.98% pure and the coating thickness was varied by changing the web speed from 0.5 to 3.5 m/min in steps of 0.5 m/min at an evaporation rate of 4–4.5 nm/s. During the evaporation process, the pressure in the chamber was maintained at $5.6–7 \cdot 10^{-4}$ Pa. The moisture content of paper substrates is typically approximately 5% under ambient conditions, thus making it difficult to achieve a high vacuum. Therefore, the paper (Metalkote 65 g/m^2; Munksjö, Sweden) was dried at 50 °C for 4 days and then at 75 °C for 3 h in a Heratherm Oven (Thermo Fisher Scientific, USA) before the aluminum coating was applied. The polymer substrate was a 50-µm polyethylene terephthalate (PET) sheet (Melinex 401; DuPont Teijin Films, UK). The evaporation rate was monitored with a QCM (008–010-G10; Inficon, USA). The positioning of the balance in the vacuum chamber is described in Section 2.2.

2.2. Model for gas cloud expansion and aluminum thickness distribution

The crucible from which the aluminum vapor expanded was positioned immediately below the roll. The thickness distribution in cross direction (CD) was estimated on the basis of geometrical assumptions by considering two factors: (a) the expected gas cloud expansion and resulting thickness distribution in CD (Fig. 3, left); and (b) the web

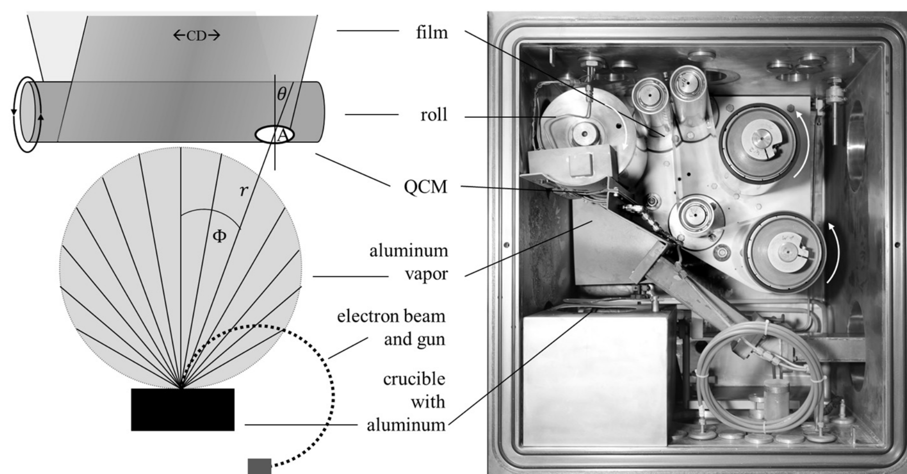

Fig. 3. Device schematic in CD (left) and an image of the evaporation chamber (right).

speed, which affects the time available for aluminum deposition in machine direction (MD) (Fig. 3, right). The aluminum thickness was related to the deposition rate, which was monitored in-line using the QCM, positioned on the right-hand side of the roll.

2.2.1. Gas cloud expansion and the resulting thickness distribution in cross direction

We assumed that the aluminum would disperse from the surface source with an angular distribution. Given that the electron beam produces a small pond of molten aluminum, the aluminum atoms are likely to originate from a small area at a constant mass evaporation rate M_e [g/s]. A certain fraction M_A would be deposited on the polymer web surface A [m^2] at distance r [m] (Fig. 3). According to Lambert's Cosine Law [35] and Martin Knudsen [36] the number of atoms evaporated per second would depend on the angle Φ between the normal and line of sight, the cosine of the angle Θ between the observer's line of sight and the normal of surface A, and a factor n related to the electron beam energy input [37] and the crucible geometry [38]. Higher energy inputs and crucibles with smaller diameters or greater depths lead to more elliptical vapor clouds, and thus a more directional deposition profile with greater thickness variations in CD. Therefore, the number of atoms, i.e. the mass flow rate M_A condensing on the surface A, can be calculated as shown in Eq. (1):

$$\frac{M_A}{A} = \frac{M_e(n+1)cos^n\phi \bullet cos\,\Theta}{2\pi r^2}. \quad (1)$$

2.2.2. Web speed and deposition time

A slit blind shielded the substrate from evaporated aluminum atoms that would impact the surface at shallow angles. The slit blind width defines the distance s in MD over which the evaporated atoms hit the polymer's surface. For a given web speed v [m/s], the aluminum can condense on a web of length s [cm] only for a certain time t [s]. Thus, the final aluminum thickness can be calculated by considering the time t and aluminum density δ as follows:

$$d = \frac{M_A}{A \bullet \delta} \bullet \frac{s}{v} = \frac{M_A}{A \bullet \delta} \bullet t. \quad (2)$$

2.3. Chemical stripping and mass spectrometry

The sample surface, volume, and dilution factors were adjusted on the basis of the expected aluminum concentration: for each sample, with a surface A of 1·10 cm^2 or 1·15 cm^2 (samples cut along MD), the aluminum was stripped off using 50, 30, 20, 10 or 5 ml of 1.0 M sodium hydroxide (Chemsolute 1.0 mol/l; Th. Geyer GmbH, Germany). The volume of 1.0 M sodium hydroxide was defined as the sample volume V. After 1 h, the liquid aluminous samples were mixed in the tubes and then diluted with double-distilled water to a dilution factor f_d of 1:10 or 2:10. The amount of aluminum in the diluted samples was then determined by mass spectrometry using an Agilent 770× ICP-MS (Agilent Technologies, USA). A standard aluminum solution (ICP multi-element standard solution IV 1.11355.0100; Merck, Germany) with an aluminum concentration of 1000 mg/l was used for calibration. This standard solution was diluted with double-distilled water to 0.10, 0.20, 0.25, 0.30, 0.50, 0.75, 1.00, 1.50, 2.00, 3.00 and 3.50 mg/l aluminum, and the calibration lines were used to correlate the given concentration with the signal intensity. This correlation was then used to calculate the concentration c [mg/l] of aluminum.

The aluminum layer thickness $d_{NOMINAL}$ for the given stripped-off sample area A was calculated on the basis of the determined aluminum concentration and by assuming a literature bulk density ρ_L value of 2.7 g/cm^3 [39]:

$$d_{NOMINAL} = \frac{c \bullet f_d \bullet V}{A \bullet \rho_L}, \quad (3)$$

and the coating weight cw [g/m^2] was calculated as

$$cw = d_{NOMINAL} \bullet \rho_L. \quad (4)$$

Values derived from ICP-MS measurements are indexed with NOMINAL hereafter and are used as reference values in this article.

2.4. Atomic force microscopy

Adhesive strips were placed on the substrate film in CD over the whole web width with a spacing of 1 m. After the aluminum coating was applied, the adhesive strip was removed to obtain a clear edge between the coated and non-coated surface parts. The measurements were performed close to the positions used for EC and OD measurements (within 1 cm^2). The measurement positions were chosen to cover a wide range of aluminum thicknesses. The accessible edge was scanned over an area of 60 μm × 60 μm with an alpha500 atomic force microscope (WITec GmbH, Germany) in pulsed force mode, with 256 points per line and 265 lines per image, with data acquired from forward and backward scans. Three height profiles were extracted for the surface at random positions perpendicular to the edge (Project Four software; WITec GmbH). The geometrical data were then exported to OriginPro (OriginLab Corporation, USA) for further calculations. The thickness of the evaporated aluminum layer was calculated from the difference in the height profiles of the coated and non-coated substrate films (Fig. 4). We ignored the peak in the middle of the profile caused when the removal of the adhesive strips lifted the aluminum layer. Two linear

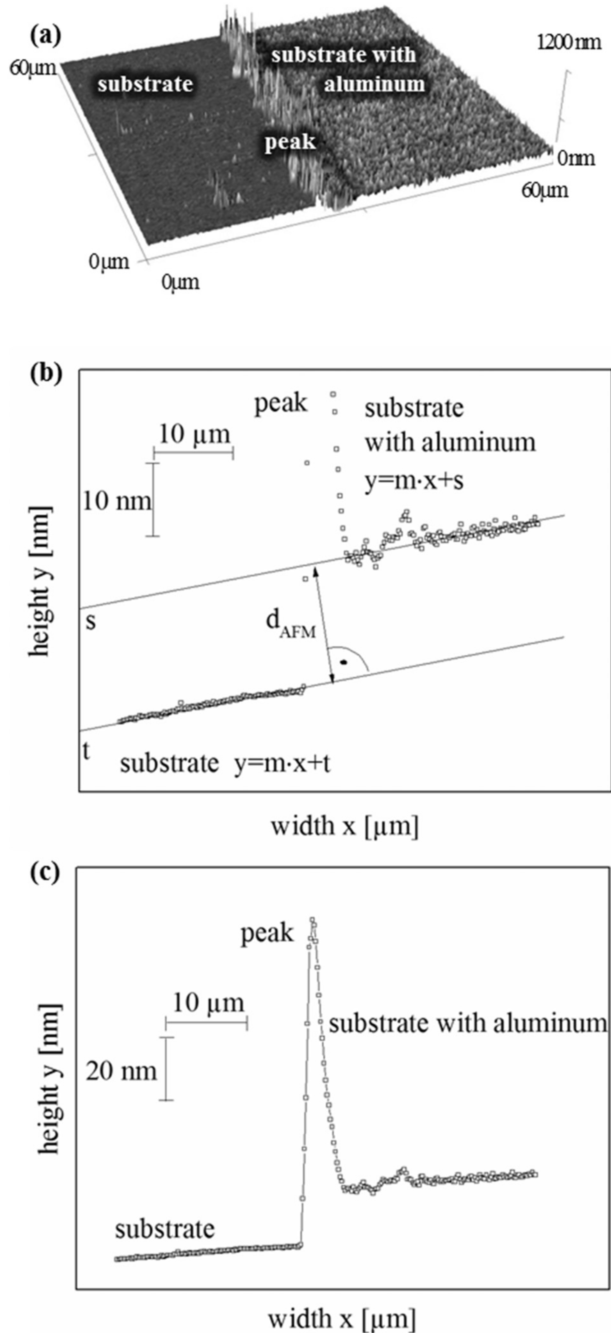

Fig. 4. Example of surface topography (a), profile extracted from it (b) and a magnified view showing the determination of d_{AFM} (c).

functions with the same slope were fitted to represent the "substrate" and "substrate with aluminum" surfaces (Fig. 3), and the thickness d_{AFM} was calculated from the normal distance between the two functions.

2.5. Optical density

The OD was measured six times within 1 cm^2 with a DDM 4 densitometer (Theimer, Germany), very close (within 1 cm^2) to the edge used for the AFM and INT measurements. For the paper substrates, the OD of the pure paper (OD = 1) was subtracted from the OD of the aluminum-coated paper. These measurements were taken under red light (absorption peak wavelength λ = 615 nm). An extinction coefficient for the deposited aluminum was assumed (k_l = 6.16) based on the linear interpolation of the literature values for k and λ (100 nm < λ < 900 nm; R^2 = 0.9894) [21,40,41]. The thickness was calculated as follows:

$$d_{OD} = \frac{OD \bullet \lambda}{k_l \bullet 4 \bullet \pi}. \tag{5}$$

The real absorption coefficient α_r was calculated from the thickness deduced by mass spectrometry $d_{NOMINAL}$ as

$$\alpha_r = \frac{OD}{d_{NOMINAL}}. \tag{6}$$

This was then used to calculate the real extinction coefficient k_r, given a light wavelength λ of 615 nm:

$$k_r = \frac{\alpha_r \bullet \lambda}{4 \bullet \pi}. \tag{7}$$

2.6. Electrical resistance

The resistance of electrical conductors depends on their geometry and electrical resistivity, which can be influenced by side-effects such as electron scattering on surfaces and grain boundaries, surface roughness, and island growth. By measuring the resistance R of aluminum while knowing length l, width b, and resistivity ρ, the thickness d can be calculated as follows:

$$d = \frac{\rho \bullet l}{R \bullet b} = \frac{\rho}{R_{\blacksquare}}. \tag{8}$$

In the 4P and 5P methods, l and b were equivalent due to the nature of the measurement setup, so they cancelled each other. The resulting resistance is called the electrical sheet resistance and is subscripted with a square ($R_{\blacksquare}$). The sheet resistance $R_{\blacksquare}$ was also determined by EC. The literature bulk value of ρ_l = 0.027 Ω·mm^2/m [39] was used to calculate the thickness.

2.6.1. Four-point probe

The experimental setup described previously [1] was used for the 4P measurements, which were carried out three times. Four copper plates were arranged (Fig. 5), and the contact areas were covered with gold. The length l and width b of the area between the inner contacts were both 10 cm. A known current was introduced over the two outer plates, and the potential difference and thus the resistance $R_{\blacksquare 4P}$ was measured over the two inner plates using a System Multimeter PM 2535 (Philips, Germany). This setup excludes the influence of the contact resistance. Values derived from 4P measurements are shown with a 4P subscript hereafter.

2.6.2. Five-point probe

The experimental setup shown in Fig. 6 was used for the 5P measurements. The distances l and b were both 10 cm. The electrode contacts were spring-loaded and covered with gold. The current was introduced via the central contact and the electrical potential, and thus the resistance $R_{\blacksquare}$, was measured by using a UT71E multimeter (TME,

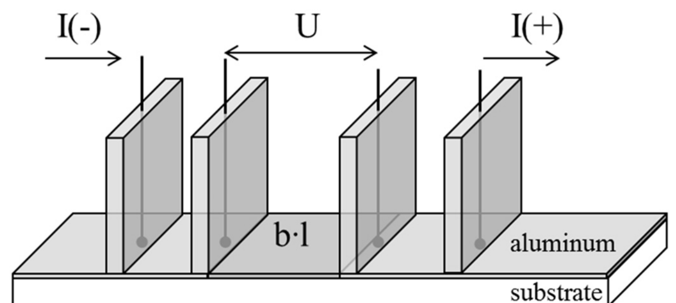

Fig. 5. Experimental setup for the four-point probe (4P).

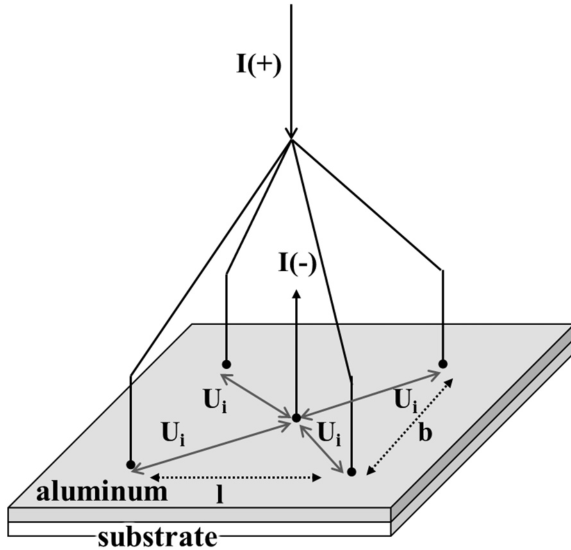

Fig. 6. Experimental setup for the five-point probe (5P).

Germany) at the outer contacts. These measurements were carried out three times. Values derived from 5P measurements are shown with a 5P subscript hereafter.

2.6.3. Eddy current

The EC measurements were performed using an EddyCus TF lab 4040 (Suragus, Germany), capturing an area of 4 mm × 5 mm. The ECs induced in the aluminum by a primary coil create a magnetic field and a current in a secondary coil, which was measured to determine the ER of the aluminum coating [12]. Values derived from EC measurements are shown with an EC subscript hereafter.

The measurements were carried out five times. For comparison with the 4P and 5P measurements, the same area of the surface was used for the EC measurements and 36 data points were acquired (Fig. 7).

The real material-specific resistivity ρ_r was calculated from the thickness $d_{NOMINAL}$ deduced by ICP-MS and the measured electrical sheet resistance $R_{\blacksquare EC}$:

$$\rho_r = d_{NOMINAL} \cdot R_{\blacksquare EC}. \quad (9)$$

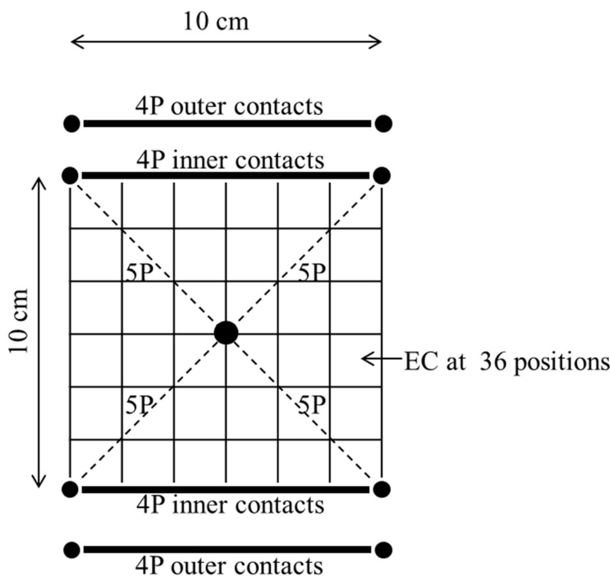

Fig. 7. Overview of the measurement area for the 4P, 5P and EC measurements.

2.7. Light interference

The INT measurements were performed as previously described [42,43] at a wavelength λ of 550 nm using a Leitz Diaplan microscope and a DFC295 digital color camera fitted with an Leitz Wetzlar F2246, 3.2/5/10 interference lens (all supplied by Leica GmbH, Germany). To achieve the same reflection and phase shift for both the aluminum coated and the non-metallized part of the PET substrate, a ~10-nm layer of gold was sputtered onto both surfaces using a Hummer JR Technics sputter system (Anatech, USA). The difference between the interference band distances a and the offset between the interference bands a' was used to calculate the aluminum thickness (d_{INT}) [nm] as follows:

$$d_{INT} = \frac{\lambda \cdot a'}{2 \cdot a}. \quad (10)$$

The measurements were carried out three times on the same samples that were used for the AFM measurements. Values derived from INT measurements are shown with an INT subscript hereafter.

2.8. Statistical methods

All data were tested against a Gaussian distribution using the Kolmogorov–Smirnov and Anderson–Darling tests, and any significant differences were tested using *t*-tests ($\alpha = 0.05$). Outlier tests were performed as specified by Hampel using Visual XSel 13.0 (CRGraph, Germany). The statistical measures we used were the arithmetic mean and standard deviation.

3. Results and discussion

Among the methods we used, only AFM and INT provide geometrical thickness data, whereas the other methods derive the thickness from measurements such as the resistance, OD, or mass of deposited aluminum. We decided to use the ICP-MS values as a reference ($d_{NOMINAL}$, $cw_{NOMINAL}$) because this technique completely dissolves the aluminum layer and the values describe the amount of pure aluminum that is physically present on the substrate surface. We adapted the model for the aluminum thickness distribution (which includes the QCM data) to the ICP-MS results for comparison, allowing the analysis and interpretation of the results generated by all the other measurement techniques, including a comparison of the three electrical sheet resistance methods. Finally, we investigated the effect of the substrate material on the measured values and determined the material constants.

3.1. Model of the angular aluminum thickness distribution (QCM) and comparison with ICP-MS values

Fig. 8 shows the dependence of the ICP-MS results, including the aluminum coating weight $cw_{NOMINAL}$ [g/m^2] and thickness d [nm], on the web speed v and position f. The reproducibility of the thickness measurements obtained via ICP-MS by QCM was examined by inserting the QCM data into the geometrical model and using the parameter n as a fit factor. In Eq. (1), all factors other than n are fixed. To determine n, $d_{NOMINAL}$ values were normalized and n was fitted to the normalized function, yielding a value of 1.6. M_A was then calculated from the deposition rate R [nm/s], QCM surface area A, and ideal density δ_{bulk} of aluminum [g/m^3] as follows:

$$M_A = R \cdot A \cdot \delta_{bulk}. \quad (11)$$

Finally, M_e was calculated by inserting the QCM values for M_A and A into Eq. (1), yielding a value of 0.0039 g/s.

The model accurately represents the angular distribution and the effect of the web speed, leading to the conclusion that the $d_{NOMINAL}$ variation in CD can be calculated on the basis of simple geometric

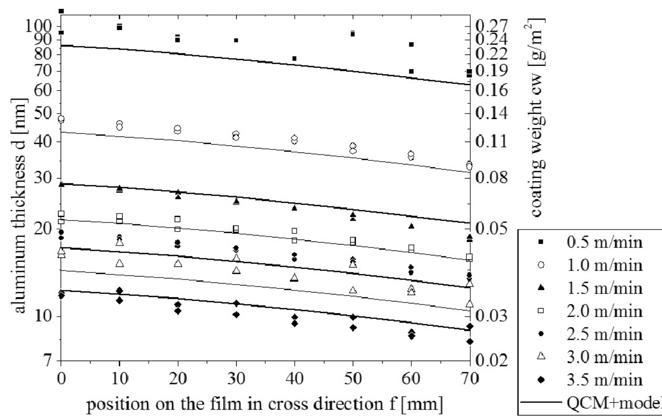

Fig. 8. Aluminum thickness comparison showing the modeled values with the factor $n = 1.6$ and ICP-MS values. ICP-MS values are well represented by the model assumptions.

assumptions and by using the QCM output values.

3.2. Comparison of the measurement techniques

Fig. 9 compares the thickness values determined using all the techniques (except 4P and 5P, which are discussed in the next section). The x-axis shows the coating weight $cw_{NOMINAL}$ and thickness $d_{NOMINAL}$ deduced from the ICP-MS measurements. Ideally, the correlation between coating weight and aluminum thickness should be linear, similar to that for $d_{NOMINAL}$. We found that d_{EC} and d_{OD} achieve high precision but low accuracy, whereas d_{AFM} and d_{INT} achieve low precision but better accuracy. Each technique is discussed in detail below.

Although neither the d_{AFM} nor the d_{INT} values were accurate, they reflected similar fluctuations and were thus internally consistent, and both measured the geometrical thickness precisely. However, the AFM values were always higher than the INT values, and this systematic difference appears to be method-dependent. We reasoned that AFM is more sensitive than INT to unevenness and peaks on the surface. The d_{INT} and d_{AFM} values fell within a range from 0.6 times lower to 1.5 times higher than $d_{NOMINAL}$. Such variations can be explained by three observations. First, both techniques are strongly affected by the aluminum surface. For the interference measurements, the surface was coated with a thin gold layer. However, the aluminum and aluminum oxide surface is not a perfectly crystalline material, hence surface roughness, gaps in the sputtered gold coating, and uneven gold layer growth all affect the recorded values [18]. Second, lower values can be explained by the proven remains of the adhesive tape on the polymer surface and waves in the polymer caused by tape removal (Fig. 10). These remains can reduce the measured geometrical thickness. Third, during the evaporation process, the deposition rate was not constant but varied by ± 8% over the course of a few seconds. The ICP-MS value represented the mean value over a larger surface (10–15 cm²), whereas AFM and INT generated very localized (< 60 μm) measurements that could vary with the evaporation rate.

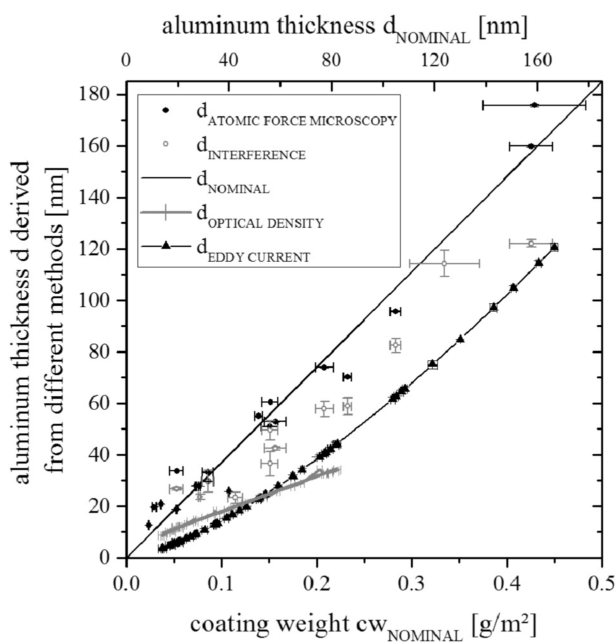

Fig. 9. Overview of the comparative results from all measurement techniques.

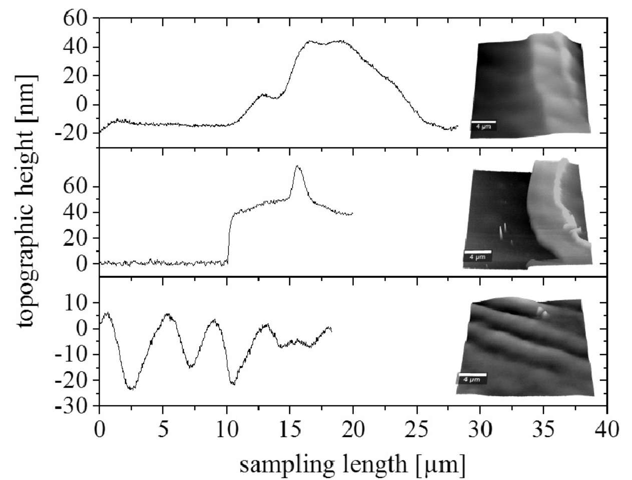

Fig. 10. Cross sections of uneven PET surface after removal of the adhesive tape.

In contrast, d_{OD} achieved very high precision. A coating weight of 0.25 g/m² corresponds to an OD of ~3.5, which is the upper measurement limit of the densitometer. At higher coating weights, the transmitted light intensity I_T becomes too low for the light sensor to measure accurately. This is why coating weights higher than 0.25 g/m² could not be measured using this technique.

The d_{EC} values were up to four times lower than $d_{NOMINAL}$, but the error decreased with increasing coating weight. The error could be caused by the insulating character of the aluminum oxide and the porosity (voids, crystallinity) of the aluminum coating. This will be discussed in more detail in Sections 3.4 and 3.5.

3.3. Comparison of the electrical measurement methods

The ER of samples with different thicknesses of aluminum on PET were measured using three different methods (4P, 5P and EC), covering the same 100 cm² surface in all cases (see Section 2.6). The thickness was calculated using Eq. (8). In Fig. 11, the y-axis shows the recorded values, whereas the x-axis shows the reference coating weight $cw_{NOMINAL}$ and thickness $d_{NOMINAL}$ deduced from the ICP-MS measurements. Ideally, the correlation between the coating weight and aluminum thickness should be linear. However, the nominal values ($d_{NOMINAL}$) were up to 3.8 times higher than the measured values on PET, although this error declined with increasing coating weight. A more detailed interpretation of this observation is provided in Section 3.5.1.

The values measured by 4P, 5P and EC were the same (significance $\alpha = 0.05$) up to a coating weight of 0.15 g/m² on PET. At coating weights > 0.15 g/m², the EC values were 30–40% higher than for 4P or 5P. These differences may reflect the varying effect of material heterogeneity on the measuring method given that microstructures are known to alter EC, 4P and 5P readings [44,45]. However, the reason for

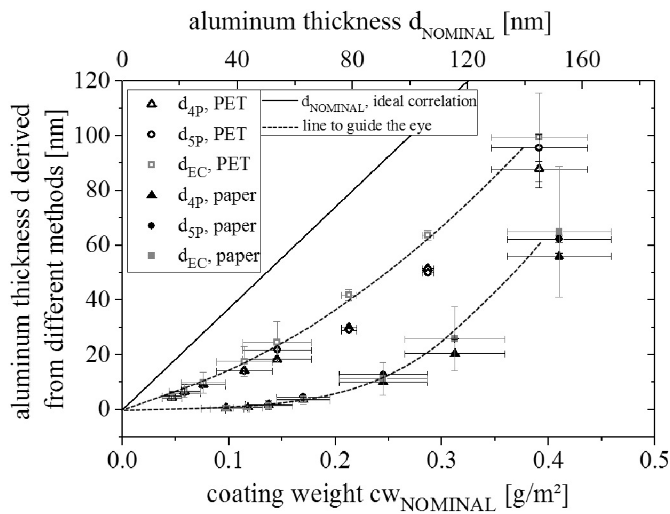

Fig. 11. Aluminum thicknesses on PET and paper as determined by 4P, 5P and EC measurements.

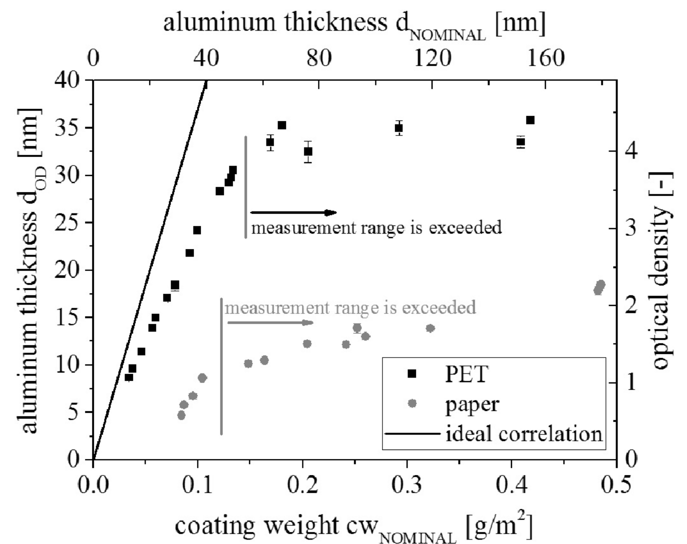

Fig. 12. Aluminum thicknesses for PET and paper substrates, from OD measurements.

the differences we observed cannot be determined based on the data we collected.

3.4. Effect of the substrate material on the measured values

3.4.1. Electrical resistance

Fig. 11 shows the thickness values obtained by EC, 4P and 5P for two different substrate materials: PET and paper. The recorded values were up to 15 times higher on PET, indicating that the same measurement technique can lead to completely different values when used on different substrates. The reason for this can be found in the structure of the aluminum coating: the typical surface roughness of PET shows nanometer-scale variations, whereas the roughness of the paper shows to variations in the micrometer range [46]. Given that nanometer-scale aluminum coatings cannot build a complete layer on such a rough surface, the coating is interrupted by voids and defects, thus leading to higher sheet resistance and lower values for aluminum thickness [47].

Surprisingly, the differences between the three measurement techniques were similar for both paper and PET, indicating that the aluminum microstructure (heterogeneity, voids and defects) cannot explain the difference between the contact and contact-free methods. Instead, the primary difference between the methods seems to be related to internal device resistances.

3.4.2. Optical density

The OD was measured for paper and PET films with various coating thicknesses as described in Section 2.5. At the same coating weight ($cw_{NOMINAL}$), the OD and thus the calculated aluminum thickness d_{OD} was up to four times higher on PET than on paper (Fig. 12). As discussed for the ER-based methods, the resulting values were dependent on the substrate or the substrate's effect on the aluminum coating structure. In this case, the micrometer-scale roughness of the paper led to defects in the aluminum coating that allowed more light to pass through, resulting in lower ODs and in turn lower derived thickness values. The uncoated paper presented a relatively high baseline (OD = 1) so the measurement limit of OD = 3.5 was reached at a lower $d_{NOMINAL}$. This explains why the OD curve for paper inclines at a lower coating weight of 0.1 g/m^2.

3.5. Determination of material constants

In the previous sections, we showed that the substrate material affects the aluminum structure, which in turn influences the material characteristics (resistivity, absorption coefficient), measured values, and deduced aluminum coating thicknesses. This agrees with earlier reports describing how the material-specific properties of thin films can deviate from the bulk properties [38,48–50]. The next step was to calculate these material constants. In each case, $d_{NOMINAL}$ was used as the reference value because it describes the total amount of aluminum available. By combining this reference value with the corresponding measured sheet resistance $R_{■}$ and OD, we were able to calculate the equivalent resistivity ρ_r, absorption α_r, and extinction k_r coefficients (see Sections 2.5 and 2.6).

3.5.1. Electrical resistivity (on PET and paper)

The electrical resistivity ρ_r was calculated using Eq. (9). As shown in Fig. 13, the resistivity cannot be assumed to be constant when using this thickness determination technique. On PET, the resistivity declined with increasing coating weight, approaching a value of ~5 μΩ·cm, which is twice the bulk value of 2.7 μΩ·cm reported in the literature [51]. The higher resistivity can be caused by electrons being deflected at grain boundaries, the random arrangement of grains, and/or the limited number of connecting paths [52]. As the coating thickness

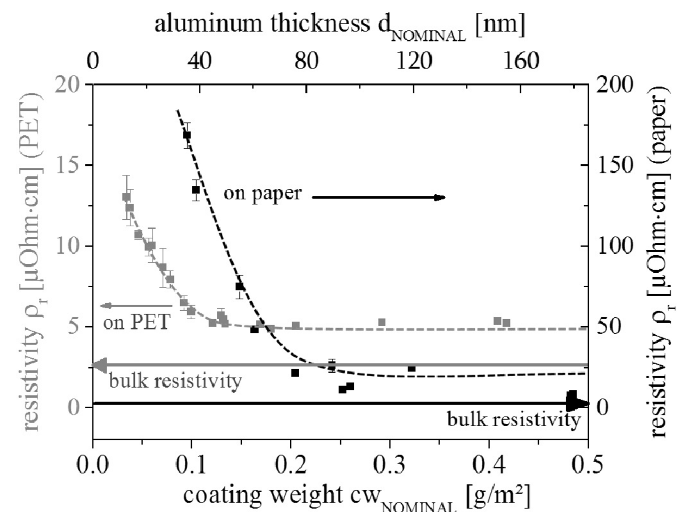

Fig. 13. Surface resistivity values for different coating weights on PET (left scale) and paper (right scale) in comparison to bulk resistivity [55]. Minimum resistivity on PET is approximately two times higher and on paper three times higher than bulk resistivity.

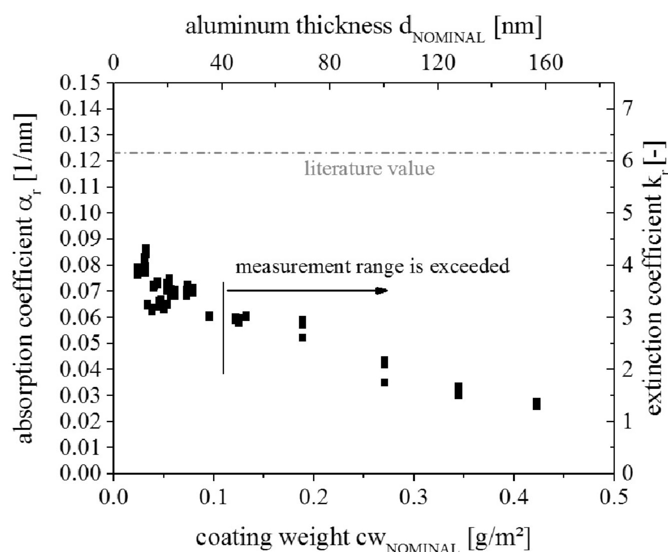

Fig. 14. Extinction and absorption coefficients for different coating weights on PET.

increases, the grain sizes increase, the connecting paths become more abundant, and there are fewer deflections, thus leading to a lower resistivity [53]. In our experiments, the minimum resistivity occurred at a coating weight of ~0.12 g/m^2, and no further improvement was achieved at higher coating weights. On paper, the surface roughness prevented the formation of a complete layer and introduced additional defects, thus increasing the resistance and resistivity. Accordingly, the resistivity values were approximately one order of magnitude higher than on PET, and minimum resistivity values comparable to those recorded on PET were only achieved at 0.5 g/m^2.

The resistivity was not constant on PET up to a thickness of 40 nm. However, 40 nm is typical for aluminum coatings that are applied in packaging applications to create gas barriers. Therefore, the use of ER to determine thickness can only be recommended if the user is aware of this error and can correct the resistivity values. Furthermore, the recorded values depend strongly on substrate roughness but can still be correctly interpreted if this factor is taken into account, e.g. by preparing calibration curves for each substrate material.

3.5.2. Extinction and absorption coefficients (on PET)

The extinction (k_r) and absorption (α_r) coefficients were calculated by introducing the measured OD and corresponding $d_{NOMINAL}$ values (Fig. 14) into Eqs. (6) and (7). The literature provides the following extinction coefficients: 4–9 for wavelengths of 0.4–0.9 μm [40], 3–21 for wavelengths of 0.3–2 μm [21], and 0–12 for wavelengths of 0.1–100 μm [41]. Linear interpolation based on these values leads to an anticipated extinction coefficient of 6.16 for a wavelength of 615 nm. The actual values we recorded are lower presumably due to the formation of transparent aluminum oxide, which reduces the absorption, and are in agreement with the value of 0.07 determined previously [1]. The coefficient values were not constant but declined slightly with increasing aluminum thickness, consistent with earlier findings Anni Lehmuskero.Markku Kuittinen.Pasi Vahimaa [21] and justified by the mass attenuation coefficient [54]. These observations show that, as with the resistivity, the absorption coefficient deviates from the literature values and also decreases as the aluminum coating becomes thicker. These effects must be taken into account in order to correctly interpret the OD values.

4. Conclusions

Our comparison of thickness determination by QCM, AFM, OD, INT and ER revealed that the methods cannot be considered redundant. The differences we observed mainly result from the assumption that the relevant material constants are equal to their literature bulk values, but this is not the case: the bulk material constants are not the same as those for thin films made from the same material because the microstructure of the deposited layer has an important effect. This means that the material constants depend on the film thickness. Furthermore, the material constants cannot even be assumed to converge on the literature values for very thick films because the layer will still include lattice defects (missing ions, foreign ions) due to the evaporation process conditions (residual oxygen, epitaxy). These conditions primarily affect the light absorption and electrical resistivity, and no general threshold thicknesses can be given where the conditions no longer have a significant effect on the measurement. The thresholds for OD, EC and AFM/INT depend on instrument sensitivity, substrate roughness, and evaporation process stability, respectively. Therefore, derived values such as material costs, gas permeation, and machine speeds can only be compared using these methods if the material-specific constants are adjusted accordingly and the values are interpreted with caution. Ideally, this should be performed for each individual process and substrate.

The AFM and INT values indicated significant thickness heterogeneity, which may be caused during sample preparation and process control management. In contrast, the EC and OD material constants (electrical resistivity and light absorption) can and must be adjusted, and this cannot be achieved simply by introducing a correction factor because resistivity in particular declines with increasing thickness and depends on the substrate. A more sophisticated model is needed to understand the relationships between substrate and resistivity and this would offer the opportunity to characterize the aluminum structure in more detail. A particularly interesting question would be how the resistivity is related to the substrate roughness, which could reveal information about defects in the aluminum structure and the anticipated gas barrier performance for packaging applications.

Author contributions

Martina Lindner wrote the paper, supervised the project, conceived and designed the experiments and analyzed the data. Florian Höflsauer and Julia Heider performed the experiments and analyzed the data. Matthias Reinelt and Horst-Christian Langowski provided critical feedback and helped shape the research, analysis and manuscript.

Conflicts of interest

The authors declare no conflicts of interest.

Funding

This research did not receive any specific grant from funding agencies in the public, commercial, or not-for-profit sectors.

Acknowledgements

The authors thank Brigitte Seifert, Daniel Schlemmer, Michael Stenger and Christine Neumeier for advice and support with the experimental work.

References

[1] H. Utz, Barriereeigenschaften Aluminiumbedampfter Kunststofffolien, Doctoral Thesis Technical University of Munich, 1995.
[2] O. Miesbauer, M. Schmidt, H.-C. Langowski, Stofftransport Durch Schichtsysteme Aus Polymeren Und Dünnen Anorganischen Schichten, Vakuum Forschung Praxis 20 (6) (2008) 32–40, https://doi.org/10.1002/vipr.200800372.
[3] M. Hanika, Zur Permeation Durch Aluminiumbedampfte Polypropylen-Und Polyethylenterephtalatfolien, Doctoral Thesis Technical University of Munich,

2004.
[4] N.J. Copeland, R. Astbury, Evaporated aluminium on polyester: optical, electrical, and barrier properties as a function of thickness and time (part I), Aimcal Technical Conference, 2010 Myrtle Beach, USA https://www.aimcal.org/2010-usa.html.
[5] T.O. Kääriäinen, P. Maydannik, D.C. Cameron, K. Lahtinen, P. Johansson, J. Kuusipalo, Atomic layer deposition on polymer based Flexible packaging materials: growth characteristics and diffusion barrier properties, Thin Solid Films 519 (10) (2011) 3146–3154, https://doi.org/10.1016/j.tsf.2010.12.171.
[6] D.J. McClure, N. Copeland, Evaporated aluminium on polyester: optical, electrical, and barrier properties as a function of thickness and time (Part I I), Aimcal Technical Conference, 2010 Myrtle Beach, USA https://www.aimcal.org/2010-usa.html.
[7] F.L. McCrackin, E. Passaglia, R.R. Stromberg, H.L. Steinberg, Measurement of the thickness and refractive index of very thin films and the optical properties of surfaces by ellipsometry, J. Res. Nat. Stan. Sec. A 67 (4) (1963) 4 (363-377).
[8] H. Chatham, Oxygen Diffusion Barrier Properties of Transparent Oxide Coatings on Polymeric Substrates, Surf. Coat. Technol. 78 (1–3) (1996) 1–9, https://doi.org/10.1016/0257-8972(95)02420-4.
[9] A. Piegari, E. Masetti, Thin Film Thickness Measurement: a Comparison of various Techniques, Thin Solid Films 124 (3) (1985) 249–257, https://doi.org/10.1016/0040-6090(85)90273-1.
[10] H.K. Pulker, Thickness Measurement, Rate Control and Automation. In Thin Film Coating Technology, (1983), Geneva, Switzerland, DOI: https://doi.org/10.1117/12.935508.
[11] D.M. Mattox, Film Characterization and Some Basic Film Properties, chap. 10, Film Characterization and Some Basic Film Properties, 1st ed, William Andrew Publishing, 1998, pp. 569–615, , https://doi.org/10.1016/B978-081551422-0.50011-5.
[12] M. Lindner, M. Schmid, Thickness Measurement Methods for Physical Vapor Deposited Aluminum Coatings in packaging applications: a Review, CoatingsTech 7 (1) (2017) 9, https://doi.org/10.3390/coatings7010009.
[13] H.A. MacLeod, Thin-Film Optical Filters, 3rd ed., CRC Press, 1986.
[14] C.A. Bishop, Vacuum Deposition Onto Webs, Films And Foils, 2nd ed., Elsevier, 2011, https://doi.org/10.1016/B978-1-4377-7867-0.00001-5.
[15] C. Lu, A.W. Czanderna, Applications of Piezoelectric Quartz Crystal Microbalances, Vol. 7 Elsevier Science, Amsterdam, 2012.
[16] E. de Hoffmann, V. Stroobant, Mass spectrometry: principles and applications, (2007), Wiley
[17] T.W. May, R.H. Wiedmeyer, A table of polyatomic interferences in Icp-Ms, At. Spectrosc. 19 (5) (1998) 150–155.
[18] K.-J. Hanszen, Der Einfluss Von Strukturunregelmässigkeiten Beim Zusammenwachsen Zweier Aufdampfschichten Auf Das Schichtdickenmessverfahren Mit Hilfe Von Vielstrahl-Interferenzen, Thin Solid Films 2 (5) (1968) 509–528, https://doi.org/10.1016/0040-6090(68)90064-3.
[19] P. Eaton, P. West, Atomic Force Microscopy, Oxford Univ, Presstime (2010), https://doi.org/10.1093/acprof:oso/9780199570454.001.0001.
[20] J. Weiss, Einflussfaktoren Auf Die Barriereeigenschaften Metallisierter Folien, 44(4) Verpakungs-Rundschau, 1993, pp. S 23–S 28.
[21] A. Lehmuskero, M. Kuittinen, P. Vahimaa, Refractive index and extinction coefficient dependence of thin Al and Ir films on deposition technique and thickness, Opt. Express 15 (17) (2007) 17 10744-10752 https://doi.org/10.1364/OE.15.010744.
[22] G. Hass, J.E. Waylonis, Optical Constants and Reflectance and Transmittance of Evaporated Aluminum in the Visible and Ultraviolet, J. Opt. Soc. Am. 51 (7) (1961) 719–722.
[23] H.D. Liu, Y.P. Zhao, G. Ramanath, S.P. Murarka, G.C. Wang, Thickness Dependent Electrical Resistivity of Ultrathin (< 40 Nm) Cu Films, Thin Solid Films 384 (1) (2001) 151–156, https://doi.org/10.1016/s0040-6090(00)01818-6.
[24] H. Hoffmann, J. Vancea, Critical-Assessment of Thickness-Dependent Conductivity of Thin Metal-Films, Thin Solid Films 85 (2) (1981) 147–167, https://doi.org/10.1016/0040-6090(81)90627-1.
[25] Y. Ke, F. Zahid, V. Timoshevskii, K. Xia, D. Gall, H. Guo, Resistivity of Thin Cu Films with Surface Roughness, Phys. Rev. B 79 (15) (2009) 155406 155406-6-155406-1 https://doi.org/10.1103/PhysRevB.79.155406.
[26] A.S. Darevskii, A.G. Zhdan, Real Structure and Electrical Conductivity of Island Films of Metals, Soviet Microelectronics 7 (5) (1978) 356–359.
[27] K.M. Leung, Electrical Resistivity of Metallic Thin Films with Rough Surfaces, Phys. Rev. B 30 (2) (1984) 647–658, https://doi.org/10.1103/PhysRevB.30.647.
[28] J.W. Lim, K. Mimura, M. Isshiki, Thickness Dependence of Resistivity for Cu Films Deposited by Ion Beam Deposition, Appl. Surf. Sci. 217 (1–4) (2003) 95–99, https://doi.org/10.1016/s0169-4332(03)00522-1.
[29] J.M. Camacho, A.I. Oliva, Surface and Grain Boundary Contributions in the Electrical Resistivity of Metallic Nanofilms, Thin Solid Films 515 (4) (2006) 1881–1885, https://doi.org/10.1016/j.tsf.2006.07.024.
[30] E.H. Sondheimer, The mean Free Path of Electrons in Metals, Adv. Phys. 1 (1) (1952) 1–42, https://doi.org/10.1080/00018735200101151.
[31] H. Heuer, S. Hillmann, M. Roellig, M.H. Schulze, K.-J. Wolter, Thin film characterization using high frequency eddy current spectroscopy, 18th IEEE International Conference on Nanotechnology, IEEE, 2009Genoa, Italy.
[32] Z. Qu, Q. Zhao, Y. Meng, Improvement of sensitivity of eddy current sensors for nano-scale thickness measurement of Cu films, NDT&E International 61 (2014) 53–57, https://doi.org/10.1016/j.ndteint.2013.09.007.
[33] J.C. Moulder, E. Uzal, J.H. Rose, Thickness and Conductivity of Metallic Layers from Eddy-Current Measurements, Rev. Sci. Instrum. 63 (6) (1992) 3455–3465, https://doi.org/10.1063/1.1143749.
[34] S. Hillmann, M. Klein, H. Heuer, In-Line Thin Film Characterization Using Eddy Current Techniques. in Studies in Applied Electromagnetics and Mechanics, STM Publishing House, Szczecin, Poland, 2011, pp. 330–338.
[35] J.H. Lambert, Photometrie: Photometria, Sive De Mensura Et Gradibus Luminis, Colorum Et Umbraee. Anding, Leipzig, Germany, W. Engelmann, 1892.
[36] M. Knudsen, Das Cosinusgesetz in Der Kinetischen Gastheorie, Ann. Phys. 353 (24) (1916) 1113–1121.
[37] D. Chaleix, P. Choquet, A. Bessaudou, L. Frugier, J. Machet, A spatial distribution study of a beam vapour emitted by electron-beam-heated evaporation sources, J. Phys. D. Appl. Phys. 29 (1) (1996) 218–224, https://doi.org/10.1088/0022-3727/29/1/032.
[38] M. Ohring, The Materials Science of Thin Films, 1st ed., Academic Press, 1992.
[39] G.E. Totten, D.S. MacKenzie, Handbook of Aluminum: Vol. 1: Physical Metallurgy and Processes, 1st ed., CRC Press, 2003.
[40] L.G. Schulz, The Optical Constants of Silver, Gold, Copper, and Aluminum. I. The Absorption Coefficient K, J. Opt. Soc. Am. 44 (5) (1954) 357–362, https://doi.org/10.1364/JOSA.44.000357.
[41] O.S. Heavens, Optical Properties of Thin Films, Rep. Prog. Phys. 23 (1) (1960) 374–376.
[42] C. Zeiss, Großes Interferenzmikroskop, Vertriebsabteilung Feinmessgeräte (1965) 1–20.
[43] H.K. Pulker, Einfaches Interferenz-Wechselobjektiv Für Mikroskope Zur Dickenmessung Nach Fizeau-Tolansky, Naturwissenschaften 53 (9) (1966) 224, https://doi.org/10.1007/bf00633891.
[44] S. Meyer, R. Gorges, G. Kreisel, Preparation and characterisation of titanium dioxide films for catalytic applications generated by anodic spark deposition, Thin Solid Films 450 (2) (2004) 276–281, https://doi.org/10.1016/j.tsf.2003.11.168.
[45] X. Ma, A.J. Peyton, Y.Y. Zhao, Eddy current measurements of electrical conductivity and magnetic permeability of porous metals, NDT & E Int. 39 (7) (2006) 562–568, https://doi.org/10.1016/j.ndteint.2006.03.008.
[46] M. Lindner, Factors affecting the hygroexpansion of paper, J. Mater. Sci. 53 (1) (2017) 1–26, https://doi.org/10.1007/s10853-017-1358-1.
[47] A.C. Siegel, S.T. Phillips, M.D. Dickey, N. Lu, Z. Suo, G.M. Whitesides, Foldable printed circuit boards on paper substrates, Adv. Funct. Mater. 20 (1) (2010) 28, https://doi.org/10.1002/adfm.200901363.
[48] D.A. Miller, Optical Properties of Solid Thin Films by Spectroscopic Reflectometry and Spectroscopic Ellipsometry, Doctoral Thesis City University of New York, 2008.
[49] O. Stenzel, Springer, The Physics of Thin Film Optical Spectra, 2nd ed., 2005, https://doi.org/10.1007/978-3-319-21602-7.
[50] K.-N. Tu, R. Rosenberg, Preparation and Properties of Thin Films: Treatise on Materials Science and Technology, 24 Elsevier, 1982.
[51] P.D. Desai, H. James, C.Y. Ho, Electrical resistivity of aluminum and manganese, J. Phys. Chem. Ref. Data 13 (4) (1984) 1131–1172, https://doi.org/10.1063/1.555725.
[52] F.M. Reicha, M.A. El Hiti, P.B. Barna, Electrical Properties of Thin Oxidized Aluminium Films, J. Mater. Sci. 26 (8) (1991) 2007–2014, https://doi.org/10.1007/bf00549159.
[53] G.P. Panta, D.P. Subedi, Electrical chracterization of aluminium (Al) thin films measured by using four-point probe method, Kathmandu Univ. J. Sci. Eng. Technol. 8 (2) (2012) 31–36, https://doi.org/10.3126/kuset.v8i2.7322.
[54] J.H. Hubbell, Photon mass attenuation and energy-absorption coefficients from 1 Kev to 20 Mev, Int. J. Appl. Radiat. Isot. 33 (11) (1982) 1269–1290, https://doi.org/10.1016/0020-708x(82)90248-4.